CrossMark

Asian monsoon variations revealed from stable isotopes in precipitation

Xiaoxin Yang[1,2] · Mary E. Davis[3] · Sunil Acharya[1,4] · Tandong Yao[1,2]

Abstract

To further our understanding of the Asian monsoon system, particularly the onset dates of monsoon sub-systems over their respective East Asian domains, we present an 8-year (2007–2014) dataset of oxygen isotopes of precipitation ($\delta^{18}O_p$) from three stations, Lulang and Nuxia in southeastern Tibetan Plateau (SETP) and Guangzhou in southeastern coastal China (SECN). The general agreement between isotopically identified monsoon onset dates with those identified by the meridional temperature gradient suggests that the initially sustained isotopic depletion is sensitive to the evolving thermal contrast between the Eurasian continent and the Indian Ocean. The 850 hPa meridional wind over nearby oceans is an efficient bridge linking isotopic variations in both regions with their respective monsoon sub-systems. The intensity of the South Asian High and tropical cyclone frequencies show stronger effects on isotopic depletion in the SECN than in the SETP and on monsoon onset timing over the South China Sea. Tibetan Plateau snow cover anomalies are significantly correlated with $\delta^{18}O_p$ in both regions on monthly timescales.

1 Introduction

The term "monsoon" refers to seasonal wind reversal and is characterized by onshore flow during summer (Wallace and Hobbs 1977). The monsoon is an important precipitation source, but in extreme cases poses threats to agriculture, industry and human livelihood. The Asian summer monsoon (ASM), which affects one-third of the world's population, is particularly pronounced in regions adjacent to the Indian

✉ Xiaoxin Yang
  xxy@itpcas.ac.cn

1   Institute of Tibetan Plateau Research, Chinese Academy of Sciences, Beijing 100101, China

2   Center for Excellence in Tibetan Plateau Earth Sciences, CAS, Beijing, China

3   Byrd Polar and Climate Research Center, The Ohio State University, Columbus, OH 43210, USA

4   University of Chinese Academy of Sciences, Beijing, China

Ocean (Wallace and Hobbs 1977). The ASM is characterized by large-scale circulation that includes several subsystems, including the South Asian summer monsoon and the East Asian summer monsoon (Conroy and Overpeck 2012; Wang and LinHo 2002), both of which have profound effects on China.

The differential land-sea thermal contrast leads to several monsoon onset phases in East Asia, although these are subject to various geomorphological features and heating conditions. The Tibetan Plateau (TP), an expansive and high-elevation land mass which is located in the mid-latitudes, has a significant impact on the ASM system. The monsoon onset over the Bay of Bengal (BOB), a consequence of the air-sea interaction, is modulated by forcing related to TP physical characteristics and the land-sea thermal contrast over south Asia during the spring season (Wu et al. 2011). Wu and Zhang (1998) demonstrated that thermal and mechanical forcing by the TP favors the ASM onset that occurs first over the BOB, which was first proposed in the early 1980s (Ananthakrishnan et al. 1983) and confirmed by more recent studies (e.g. Lau and Yang 1996; Mao et al. 2011; Wu et al. 2011; Wu and Zhang 1998).

The monsoon system over the TP is governed by complex processes. The vast cryosphere, which in total is the largest ice mass outside the Arctic and Antarctica, also serves as a reservoir for both water and energy which interacts with the ASM circulation. Xie et al. (2005) described a negative correlation between TP snow cover and the subsequent East Asian Summer Monsoon as determined by western North Pacific typhoon frequency and the number of typhoon landfalls in China. Changes in the snow cover, along with changes in surface albedo and thereby sensible heating, also modulate the atmospheric circulation over the TP (Wu and Kirtman 2007; Xu et al. 2009). Monsoon variability has been characterized using various methods, including the all Indian summer rainfall index based on the Indian Meteorological Department stations (e.g., Parthasarathy et al. 1992), physical proxies based on reanalysis data [e.g., time-mean zonal wind shear (Webster and Yang 1992), meridional wind shear (Goswami et al. 1999), area averaged negative OLR anomalies (Wang and Fan 1999), tropospheric temperature gradient (Xavier et al. 2007) and meridional temperature gradient (Mao et al. 2011)], and theoretical models for atmospheric general circulation (e.g., Lau and Yang 1996). However, it should be noted that monsoon variation may not be the sole determinant of precipitation intensity, as the increase in atmospheric moisture in a warmer climate would also affect the frequency of precipitation events, even if atmospheric circulation remains the same (Trenberth 2011). Thus the identification of monsoon variability by precipitation distribution and intensity might be supplemented by physical processes analysis associated with monsoon circulation. Many investigators have attempted to understand ASM variability using that methodology (Goswami and Jayavelu 2001; Wang et al. 2004a, b; Webster and Yang 1992).

Stable isotopic ratios are highly influenced by atmospheric physical processes and are widely used to reconstruct atmospheric circulation (Liu et al. 2008; Yao et al. 2013). Since 1961 the Global Network of Isotopes in Precipitation has yielded valuable data which have enhanced our understanding of the effects of meteorological parameters (precipitation, temperature, air circulation) and atmospheric kinetics on stable isotopic ratios (Araguas-Araguas et al. 2000; Dansgaard 1964; Sengupta and Sarkar 2006). In addition, a network of stations has been established across the TP (the Tibetan Network for Isotopes in Precipitation, or TNIP) to obtain samples from precipitation events for stable isotope analysis and to take measurements related to atmospheric circulation (Yao et al. 2013). These data have been used to delineate the northern limit of monsoon intrusion on the TP (Tian et al. 2001) and to categorize the three major atmospheric circulation domains (Yao et al. 2013).

Determining the timing of the monsoon onset is important as it is essential for agricultural and societal development. The Coupled Model Intercomparison Project Phase 5

projects a weakening of the Indian summer monsoon circulation in an increasingly warm climate, which is nevertheless accompanied by increasing precipitation that is largely attributed to increased atmospheric moisture content (Trenberth 2011; IPCC 2013). Multiple indices to characterize the monsoon that incorporate various atmospheric circulation features have been proposed, yet a well-defined or widely accepted index remains elusive (Wang et al. 2004a, b). The isotopic composition of precipitation has the potential to provide an alternative means to address this issue, since such data contain information on the atmospheric processes associated with precipitation.

Data from TNIP have been used to identify temporal monsoon variations, i.e., an earlier summer monsoon onset over the Bay of Bengal than over the South China Sea (Yang et al. 2012b).Here we discuss new results that build on that study, using ground observations that are essential for verifying the performance of model simulations which provide credible explanations of physical mechanisms of monsoon processes and help improve projections of future scenarios (IPCC 2013). Our primary objectives are to address the onset timing of the Asian monsoon sub-systems in this region over the last decade using the oxygen isotopic values of precipitation ($\delta^{18}O_p$), and to verify the characteristic isotopic signals of monsoon variations by considering multiple atmospheric and oceanic impacts on $\delta^{18}O_p$. We use $\delta^{18}O_p$ data from samples collected daily from 2007 to 2014 to investigate monsoon variability, which is verified using reanalysis data. We discuss factors affecting $\delta^{18}O_p$ and explore the role of those factors in the isotopic signal of the monsoon initiation.

2 Sampling and data processing

For event precipitation sampling at Lulang (LL) and Nuxia (NX) in the southeastern TP, and at Guangzhou (GZ) on the southeastern coast of China (Fig. 1), we received cooperation from the local meteorological stations at NX and GZ and the Chinese Academy of Sciences' field station in the southeastern TP (Table 1). All these stations are manned in shifts around the clock to ensure continuous operation of manual and automatic equipment. Because of the high relative humidity and the necessity for high sampling frequency during summer months, the sampling procedure included the use of deep buckets with plastic bag inserts at all collection points. Samples were collected immediately after each event and poured into 15 ml polyethylene bottles which were tightly capped before being placed in cold storage at the stations. Note that each precipitation event yielded only one bottle of sample that was filled as much as possible. Snow samples were allowed to melt at room temperature before being poured into bottles. The humid environment, immediate collection and cold storage facilities ensured minimal
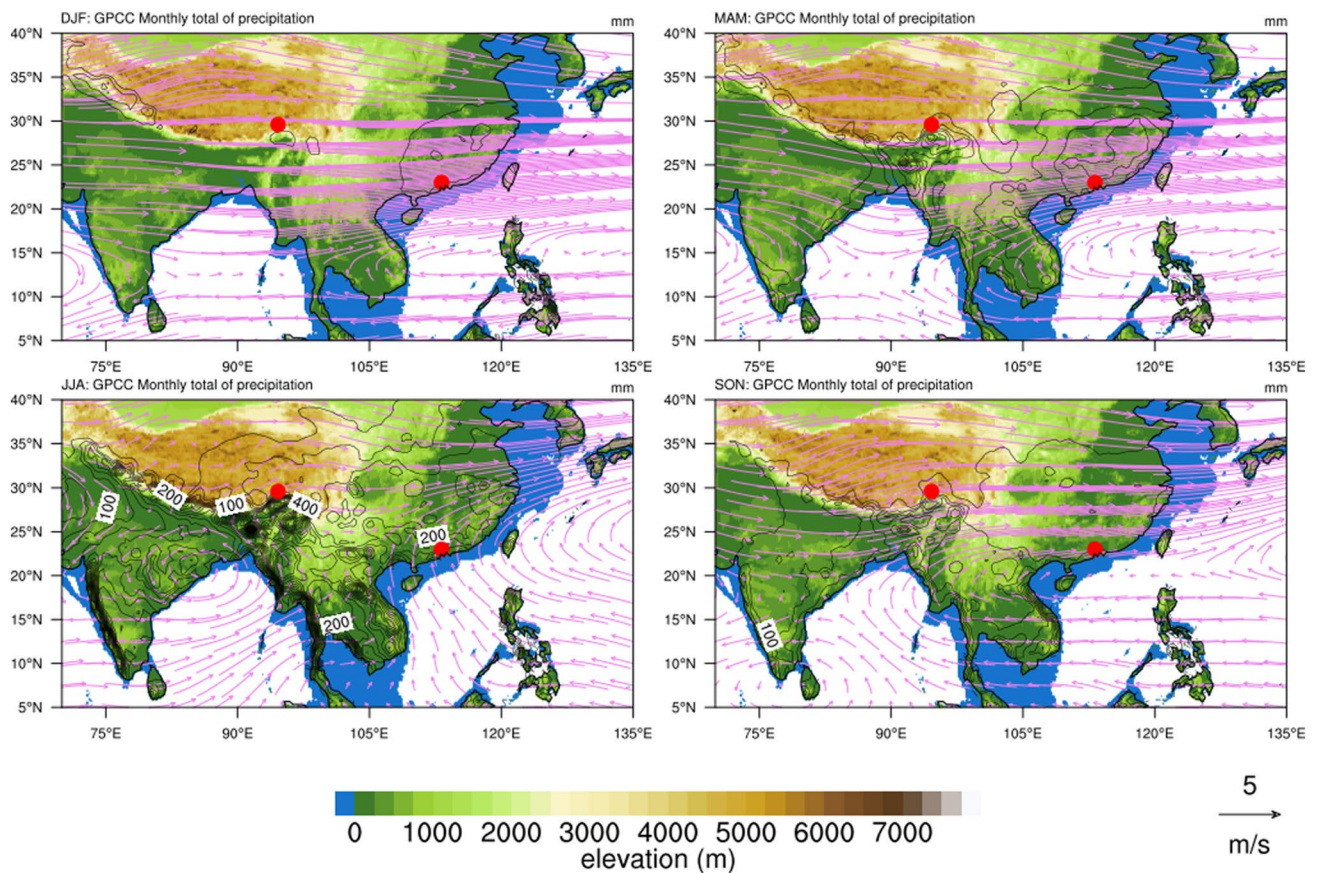
Table 1 Locations and sampling periods at the three stations in this study

	Longitude (°E)	Latitude (°N)	Altitude (m.a.s.l)	Sampling start	Sampling end	Number of spls
GZ	113.32	23.13	7	Jan. 2007	Dec. 2014	1755
LL	94.73	29.77	3330	Jan. 2007	Jun. 2014	731
NX	94.65	29.47	2920	Jun. 2009	Oct. 2014	594

post-sampling evaporation. Each bottle was marked with the collection date, thus allowing verification and calibration with real-time meteorology data which include surface temperature (T) and precipitation amount (P) at both the start and end of each event. Samples were transported to Beijing every 10 months for analysis at the Chinese Academy of Sciences Key Laboratory of Tibetan Plateau Climate Change and Land Surface Processes.

Measurements were made with a Picarro Li-2102 analyzer using a cavity ring-down system at an analysis rate of 45–55 samples per batch, not including standard samples. Three secondary standards of comparatively higher, lower and identical isotopic compositions with respect to sample values are used in our measurements, with the sample of identical isotopic composition as the main standard (Table S1). All the standard samples are tested against the Vienna Standard Mean Ocean Water and are selected based on our empirical knowledge of the isotopic composition of measured samples in the region. Details of the isotopic ratios of the standard samples are provided in the supplementary information. The measurement errors (i.e., standard errors of measurements of the main standardsamples) are $\pm 0.1‰$ for $\delta^{18}O_p$ and $\pm 0.5‰$ for hydrogen isotopes of precipitation (δD_p). To examine the data quality, d excess values (calculated as d excess $= \delta D\text{-}8 \times \delta^{18}O_p$) were used to identify outliers [i.e., absolute values surpassing 40 (Wushiki 1993)], which were discarded to avoid possible biases. In this way we eliminated three outliers

from the GZ site and six outliers from the NX site. Since these nine samples accounted for a negligible percentage of the total number of samples (Table 1), their removal had little effect on our statistical analyses. To better delineate the stable isotope values associated with the weather conditions, the event precipitation isotopic data was processed as daily amount weighted values, which were then used to calculate monthly amount weighted means and anomalies.

We created a composite time series of the data from the nearby LL and NX stations in order to compensate for the 6-month difference in collection period between GZ and LL. This composite is feasible not only because of the proximity of LL and NX (Table 1), but also because of the high number of simultaneous precipitation events (over 50% of precipitation days occurred at both localities between 2009 and 2014), and similar isotopic seasonality (Fig. S1). A caveat to this procedure is the > 400-m difference in altitude between LL and NX which may introduce an "altitude effect" on the stable isotopes. We account for this difference by using the lapse rate of − 0.30‰/100 m in the southeastern TP (Yang et al. 2012a) to calibrate the daily isotope data for the lower-elevation station at NX before merging them with the data from LL. Therefore, the following discussion will focus on daily and monthly data from GZ in southeast China (referred to as SECN below) and the LL and NX data composite from the southeastern TP (SETP) region.

To investigate the monsoon variability based on the isotopic records and explain the mechanisms for those variations, we use observation-based monthly precipitation data from the Global Precipitation Climatology Project (GPCP) full data reanalysis Version 7 (1.0° × 1.0°), along with the Global Precipitation Climatology Center (GPCC) monitoring dataset since 2014 (Adler et al. 2003). Long-term (1981–2010) averaged wind circulation, monthly zonal and meridional wind anomalies, monsoon indices and 200 hPa geopotential heights are derived from NCEP/NCAR Reanalysis 1 data (2.5° × 2.5°) (Kalnay et al. 1996). Atmospheric reanalysis data, including zonal and meridional wind velocities, specific humidity and surface pressure, as well as vertical integral products are obtained from the ERA-Interim acquired from the European Centre for Medium-Range Weather Forecasts. We also use uninterpolated outgoing longwave radiation (OLR) data provided by NOAA/OAR/ESRL PSD from http://www.esrl.noaa.gov/psd/. In light of the significant presence of tropical cyclones in both regions, we utilize a time series of tropical cyclone events provided by the Joint Typhoon Warning Center. The Eurasian snow cover data is provided by the Rutgers Global Snow Lab (Robinson et al. 2012) and the Tibetan Plateau snow cover data by Shen et al. (2015).

3 Results

3.1 $\delta^{18}O_p$ seasonality and climatic controls

Precipitation in both study regions shows significant monsoon characteristics. In the SETP (SECN) 67.2% (52.4%) of the annual total occurs from June to September. During the study period (2007–2014) daily $\delta^{18}O_p$ data show noticeable intra-seasonal similarities which are characterized by monsoon ^{18}O depletion and pre- and post-monsoon ^{18}O enrichment (Fig. 2a, b). The daily $\delta^{18}O_p$ time series in the SECN shows a decreasing trend from May to September (Fig. 2a), while the SETP data show a significant decrease from June to October (Fig. 2b). Their common period of isotopic depletion (June–September) is accompanied by heavy monthly precipitation, which broadly agrees with the meteorological definition of the Asian summer monsoon period (Qian and Yang 2000; Wang et al. 2004a, b).

Many studies (Johnson and Ingram 2004; Liu et al. 2014) also report the dominant influence of the amount effect in this region. However, the high temporal resolution of our sampling allows an unprecedented evaluation of the atmospheric controls on isotopic values on a monthly basis. Despite the dominant precipitation amount control over $\delta^{18}O_p$ in the SECN within each month (Fig. 2c), the temperature effect is also significant from May to September, with the $\delta^{18}O_p$–T gradient varying from 0.16‰/°C in May to 0.48‰/°C in July (Fig. 2c). Also notable is the significant amount effect from December to February, despite the low monthly precipitation (Fig. 2a, c), during a period when weak positive $\delta^{18}O_p$–T correlations are observed (Fig. 2c). The convection organization (Kurita 2013), along with the indirect influence of downdraft recycling (Risi et al. 2008), are proposed as possible drivers of the amount effect. The mesoscale convective systems (e.g. monsoon circulation) during the summer half year thus lead to fluctuations in the condensation level with organized convection, resulting in in-phase variation under Rayleigh fractionation of the $\delta^{18}O_p$ values with the cloud base temperature. During the winter half year, downdraft recycling is enhanced by a deficient moisture supply (Risi et al. 2008), leading to high isotopic ratios in corresponding precipitation that is mainly a function of local evaporation (Johnson and Ingram 2004). The occurrence of temperature and amount effects in different seasons has also been reported previously (Yang et al. 2011). Here we reiterate that different moisture sources and trajectories play a major role in isotopic variations in the region.

In comparison, significant (p < 0.05) correlations between temperature and $\delta^{18}O_p$ in the SETP are observed only in April ($\delta^{18}O_p$–T gradient = 0.41‰/°C), August
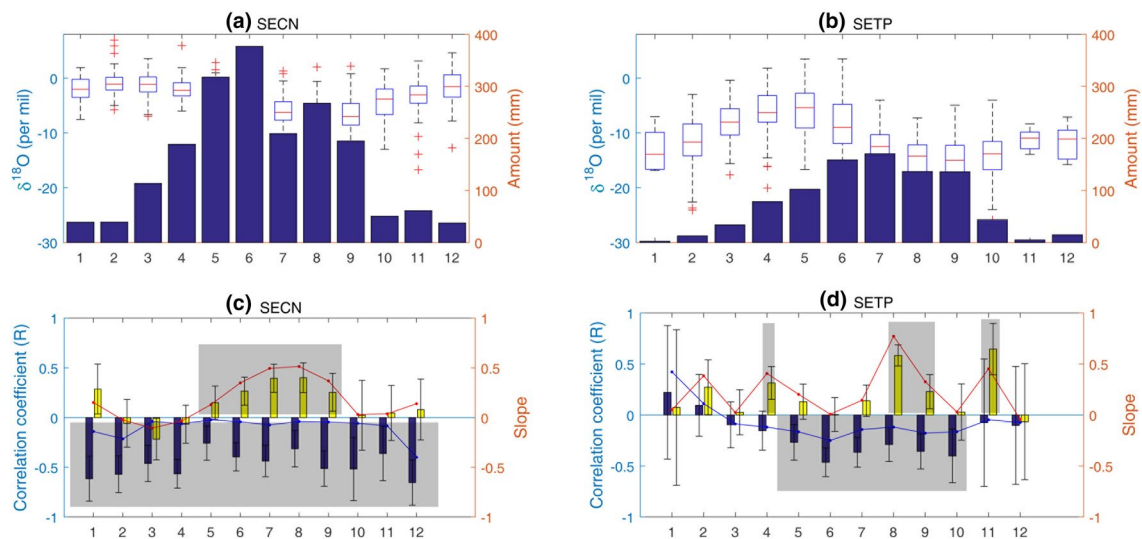
Fig. 2 Box-whisker plots of intra-seasonal variations of $\delta^{18}O_p$, and local temperature (T) and precipitation (P) controls over $\delta^{18}O_p$ based on daily data during the 8-yr period in both regions. **a** Box plot of $\delta^{18}O_p$ (whiskered boxes) within each month and corresponding 8-year mean monthly precipitation amount (solid bars) in the SECN; **b** same as **a**, but for the SETP. For each whiskered box, the central mark is the median, the edges of the box are the 25th and 75th percentiles, the whiskers extend to the most extreme data points the algorithm does not consider as outliers, and the outliers are plotted individually as red plus symbols. **c** Correlation coefficients (R-value) and slopes of the least square linear regressions with respective error bars at 95% confidence level for the $\delta^{18}O_p$-T (yellow bars and blue curve) and $\delta^{18}O_p$-P correlations (blue bars and red curve) in the SECN; **d** same as **c**, but for the correlations in the SETP. Significant correlations are shaded gray in **c** and **d**

(0.77‰/°C), September (0.33‰/°C), and November (0.45‰/°C), while the correlations between precipitation amount and $\delta^{18}O_p$ are consistently significant only during the summer half year (May–October) (Fig. 2d). The dominance of the amount effect on a daily basis in the SETP has been reported previously (Yao et al. 2013); here for the first time we detail a significant temperature effect in the region only during certain months. Local evaporation is the dominant moisture source prior to and shortly after the monsoon process, while organized convection reaches maximum strength during monsoon maturation from August to September.

This interpretation of a significant temperature effect in monthly precipitation in both monsoon domains represents a departure from previous studies. Local temperature has previously been thought to be the overriding control on isotopic values (Yurtsever et al. 1975), as temperature determines the fractionation factor that directly controls the isotopic composition in precipitation (Gat et al. 1996). Therefore, the presence of the temperature effect and its implications in the monsoon domains warrant further study.

3.2 Intra-seasonal variation of the local meteorological water lines

The local meteorological water lines (LMWLs) show different intra-seasonal features in both regions. In the SECN, LMWL slopes and intercepts vary in phase from June to October (Fig. 3a). On the other hand, in the SETP the slopes and intercepts vary in phase throughout the year, with the highest slope in January, and the lowest slopes (< 8) in June–October (Fig. 3b). The covariance of slope and intercept in the SETP data is interesting to note. LMWL slopes are determined by fractionation factor and precipitation mechanisms, while their intercepts are indicative of moisture source temperature (Gat 2005). Here, the covariance suggests a close correlation between fractionation mechanisms and temperature of precipitation during monsoon seasons in both regions, but in the SETP the correlation is even more consistent throughout the year.

D-excess varies regionally with humidity, wind speed (Benetti et al. 2014) and sea surface temperature during primary evaporation (Clark and Fritz 1997), and contains information about moisture source conditions (Gat et al. 1996). A negative correlation between d-excess and $\delta^{18}O_p$ suggests kinetic fractionation (Froehlich et al. 2008), and is associated with sub-cloud evaporation due to the increasing distance between the surface and the cloud base during monsoon convection and lifting of the condensation level. In the SECN marine modulation of the condensation level and temperature is intense throughout the year, leading to significant correlations between d excess and $\delta^{18}O_p$ in all months except October (Fig. 3c). However, in the SETP the monsoon related feature characterized by the negative d excess-$\delta^{18}O_p$ correlation is significant only during July–September (Fig. 3d), and is more seasonally defined (Fig. S2),
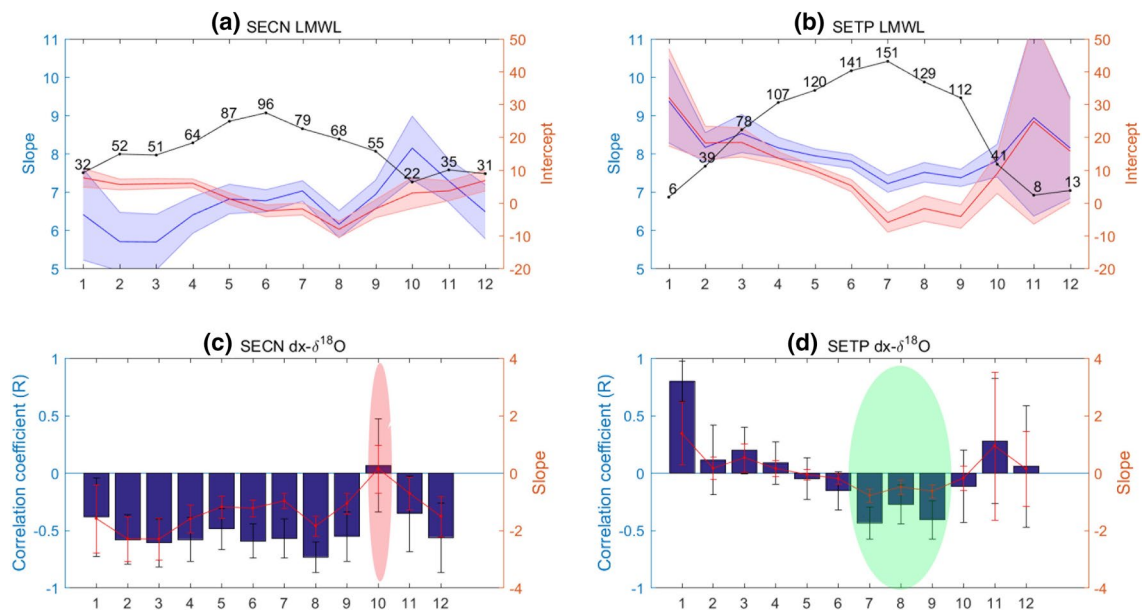
Fig. 3 Variations of LMWL and d excess-δ^{18}O correlations within each month based on daily data during the 8-years period in both regions. **a** LMWL slopes (blue) and intercepts (red) enveloped by each of their mean±1 standard deviations in the SECN, with numbers of samples (black dotted curve) for each month; **b** same as **a**, but for the SETP. **c** Correlation coefficients (dark blue bars) and slopes (red curve) with their respective error bars at 95% confidence level for the d excess-δ^{18}O correlations within each month in the SECN; **d** same as **c**, but for the SETP. Red shading in **c** highlights the month when the correlation is not significant (p > 0.05), while green shading in **d** highlight months when the correlations are significant (p < 0.05)

as negative d excess-$\delta^{18}O_p$ correlations exist in the SETP in summer (R = − 0.16, n = 421, p < 0.01) and fall (R = − 0.21, n = 161, p < 0.05) of the four seasons.

4 Discussion

4.1 Monsoon variations revealed from daily $\delta^{18}O_p$

The SETP is affected by the Bay of Bengal branch of the monsoon component of the South Asian Summer Monsoon, while the SECN is influenced by the South China Sea monsoon (Qian and Yang 2000) which is part of the East Asian Summer Monsoon system (Conroy and Overpeck 2012; Wang and LinHo 2002). Both these large-scale systems are initially driven by significant contrasts in heat capacity between the ocean and land, which sets up strong sea breezes at the beginning of the boreal summer.

We propose using isotopic data from 2007 to 2014 from the LL and NX composite as representative of SETP and GZ as representative of SECN to identify the onset of each sub-monsoon system (Yang et al. 2012b) (Fig. 4a). Monsoon onset is isotopically identified after meeting the following two criteria: (1) the amount-weighted average of daily δ^{18}O ($\delta^{18}O_{wt}$) in March in each respective year is taken as a threshold, and (2) the monsoon initiation is marked from April onward by days with a below threshold $\delta^{18}O_{wt}$ for 4

continuous days within a 7-day period. Such criteria consider the deep convection during monsoon onset and the stability of cyclonic circulation dominance once the monsoon is initiated. A case study to validate the isotopic criteria against the meteorological criteria for monsoon onset is provided in Yang et al. (2012b).

Following the aforementioned criteria, the onset of the Bay of Bengal monsoon in the SETP ranged from April 22 in 2007 to June 28 in 2009, while the South China Sea monsoon onset ranged from April 1 in 2010 to June 25 in 2009. In 2007 and 2012, both the Bay of Bengal and South China Sea monsoons commenced on the same date in late April, the earliest in our record, with the 2012 onset date being the earliest in our record. In 2009 the monsoon initiation date for both regions occurred at the end of June, the latest in our record for either region. A transition in the onset dates of the two sub-monsoon systems is noticeable. In 2008, the Bay of Bengal monsoon commenced (April 28) earlier than the South China Sea monsoon (May 18), consistent with our previous findings. This was associated with the surface sensible heating of the TP and the resulting displacement of the South Asian High (Liu and Wu 2004; Wu et al. 2015). Since 2009, however, daily $\delta^{18}O_p$ variations show a late onset of the Bay of Bengal monsoon compared with the South China Sea monsoon, with exception of 2012 as discussed above (Fig. 4a). Verification has been performed using 850 hPa wind and daily OLR reanalysis data for the onset date ± 5
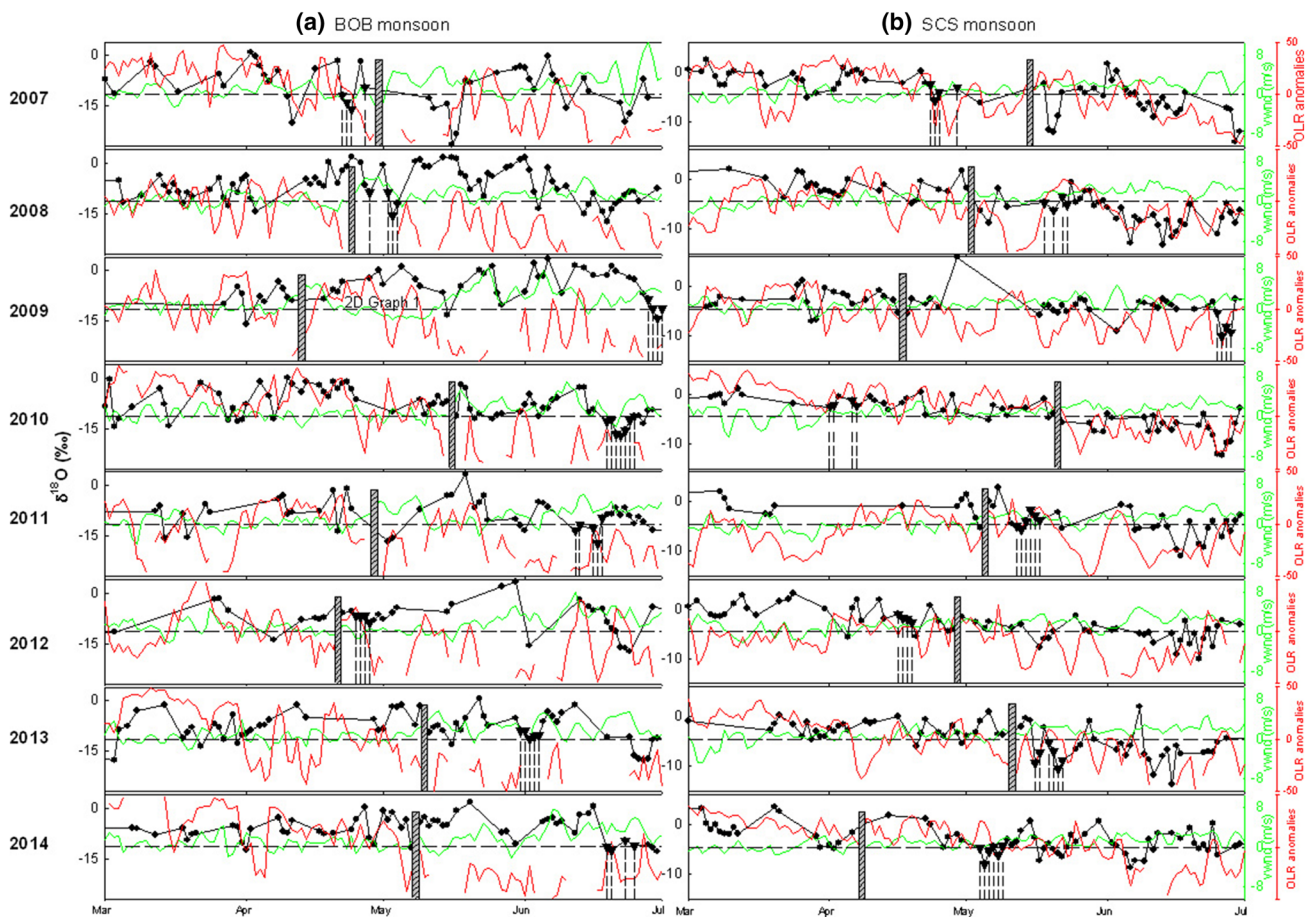
Fig. 4 Identification of summer monsoon onset based on daily variation of $\delta^{18}O_p$ (black dotted curves) and corresponding OLR (red curves) and meridional wind (green curves) over **a** the Bay of Bengal (5–21°N, 80–100°E), which affects the SETP and **b** over the South China Sea (5–21°N, 105–125°E), which affects the SECN. The monsoon onset identified by $\delta^{18}O_p$ is marked by gray dotted lines, while the onset identified by the atmospheric meridional temperature gradient is marked by gray hatched columns. The onset date for each individual year is defined as the day when: (1) the area-averaged upper tropospheric (200–500 hPa) MTG on the eastern Bay of Bengal (5–15°N, 90–100°E) changes from negative to positive, and (2) the MTG remains positive for more than 10 days (Mao et al. 2011)

days (as circulation on synoptic scales is usually presented as pentads), which demonstrates a northerly to southerly prevailing wind shift together with low OLR (suggestive of strong convection) in each region during the period of monsoon commencement (Fig. 4).

Comparisons of monsoon onset dates identified by $\delta^{18}O_p$ with those identified by the meridional temperature gradient (MTG) (Mao et al. 2011; Wu et al. 2011) highlight the general similarity between them in 2007–2008 and 2012 for the SETP and in 2008 and 2010–2012 for the SECN, as well as the noticeable differences in other years. It is difficult to determine which criteria are more reliable in revealing the first signs of monsoon onset, as they alternate with the coincidence of transition in meridional wind and OLR. Considering the Bay of Bengal monsoon onset in 2009 as an example, the monsoon onset was identified by MTG as April 16, yet at that time OLR values were high (> 235 W/m²) and southerly winds were weak. We concede that the onset dates

determined by our isotopic criteria may occur later during certain years such as 2009–2010 and 2014, which may have been associated with the development of El Niño Southern Oscillation (ENSO) conditions (ENSO years are identified by the Center for Ocean–Atmosphere Prediction Studies at http://coaps.fsu.edu/jma). Yet the comparatively late monsoon signal in daily $\delta^{18}O_p$ is understandable as our isotope data are based on precipitation events, while the marine onset dates must precede monsoon precipitation at inland locations. In addition, meso-scale atmospheric circulation (e.g. cyclonic circulation) prior to the advent of the monsoon may disturb moisture generation at the ocean source, thus deferring the normal course of the monsoon. Still, monsoon onsets identified by daily $\delta^{18}O_p$ at the monsoon front are generally consistent with those identified by reanalysis data over the oceanic source region.

Inter-annual variations in monsoon onsets identified by the isotopic criteria demonstrate diverse trends for the two
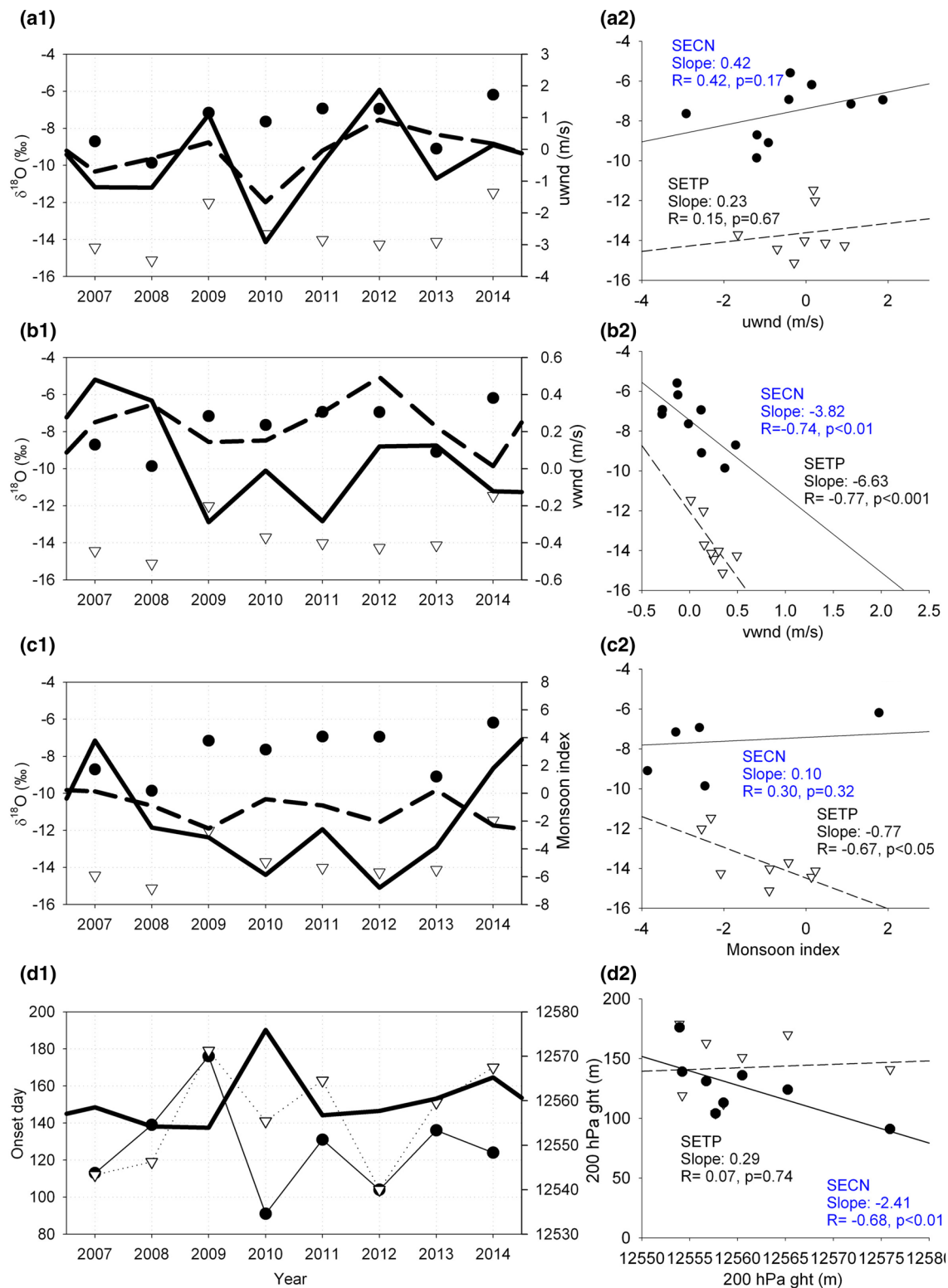
sub-monsoon systems, with gradually delayed emergence in the SETP indicative of weakening monsoon over the BOB while advancement in the SECN is suggestive of strengthening monsoon over the South China Sea (Fig. S3a). Actually, the inter-annual variations in precipitation amounts in the

two regions during June–August also show reversed trends after 2010 (Fig. S3b). Such variations occur under climate scenarios featuring the weakening of the South Asian Summer Monsoon (Singh 2016) and comparative strengthening of the East Asian Summer Monsoon (IPCC 2013). This

◄**Fig. 5** Inter-annual variations in June–August monsoon parameters from 2007 to 2014 compared with June–August amount-weighted $\delta^{18}O_p$ in the SETP (white triangles) and SECN (black dots) for **a1** and **a2** June–August zonal wind (uwnd) velocity anomalies at 850 hPa, **b1** and **b2** the 850 hPa meridional wind (vwnd) anomalies, over the Bay of Bengal (black broken curve; 5°N–21°N, 80°E–100°E), and the South China Sea (black solid curve; 5°N–21°N, 105°E–125°E); **c1** and **c2** the East Asian summer monsoon index (black solid curve; calculated as the June–August sea level pressure difference between 160°E and 110°E from 10°N to 50°N (Guo 1983; Zhou et al. 2009) and the Indian summer monsoon index (black broken curve; calculated as the meridional differences between the June–August 850 hPa zonal winds averaged over 5°N to 15°N, 40°E to 80°E, and 20°N to 30°N, 60°E to 90°E (Wang et al. 2004a, b); **d1** 200 hPa geopotential height over an area bounded by 24°N–28°N and 70°E–90°E compared with the onset day in each year; **d2** the correlations between the 200 hPa geopotential heights and respective monsoon onset days in each calendar year. Illustration of both monsoon indices can be found in Figure S4 in the supporting information. The zonal and meridional winds, as well as both monsoon indices, are normalized to their respective 1986–2005 averages

highlights the potential for $\delta^{18}O_p$ to serve as an alternative means to study the complex Asian monsoon system. The following sections explore the mechanisms that likely influence the links between monsoon circulation and $\delta^{18}O_p$ variation at the monsoon front.

4.2 Possible links between monsoon circulation and isotopic variations during monsoons

To explore possible linkages between monsoon circulation and isotopic variations, we studied the inter-annual variations of various circulation parameters, including zonal and meridional winds over the respective moisture sources for the study regions, meteorological monsoon indices and high-level geopotential heights representative of the South Asian High intensity (Wu et al. 2015) (Fig. 5). Although our isotopic data are of event resolution, correlations of the monthly $\delta^{18}O_p$ values with the monthly, rather than daily, reanalysis data are examined here, as monsoon evolution is a climatic phenomenon while daily values may fluctuate due to noise from daily synoptic phenomena.

The correlations between isotopic compositions in both regions and the 850 hPa June–August zonal wind are not significant, especially for the SETP (Fig. 5a1, a2). Little direct effect is inferred on $\delta^{18}O_p$ in the East Asian monsoon front by the zonal wind circulation over the moisture source on the monsoon front in East Asia. On the other hand, $\delta^{18}O_p$ in both regions during June–August show significant negative correlations with 850 hPa meridional winds over their respective marine moisture sources (p < 0.05; Fig. 5b). As both regions lie to the north of their moisture sources, the strong correlation with the southerlies throughout the observation period indicates prevailing onshore flow from respective oceanic zones adjoining the study regions. The

southerly winds thus bridge the isotopic variations in both regions with monsoon circulation process, as higher (lower) velocity southerlies coincide with more depleted (enriched) $\delta^{18}O_p$ during June–August. Lower meridional wind velocities in 2009 and 2014 may be indicative of weakening of the bridge linking large-scale circulation with local precipitation. This also implies longer transport time for the oceanic moisture to reach the continent and thus a much later signal of monsoon onset in daily $\delta^{18}O_p$. In addition, corresponding $\delta^{18}O_p$ values in both these years are high, suggesting significant interaction of local process with the large-scale atmospheric circulation.

The different responses of regional $\delta^{18}O_p$ to larger scale circulation are also noticeable. A robust negative correlation (p < 0.05) is observed only between $\delta^{18}O_p$ in the SETP and Indian summer monsoon intensity (R = −0.67) (Fig. 5c2), suggesting a higher level of dominance of the South Asian Summer Monsoon over the SETP than the East Asian Summer Monsoon over the SECN. The lack of significant correlation between $\delta^{18}O_p$ in the SECN and the East Asian Summer Monsoon is likely linked to meridional shifting of the Intertropical Convergence Zone, the seasonal shift of which leads to active convergence and convection off the southeast coast of China which results in a multitude of moisture sources subject to different trajectories and formation mechanisms.

The South China Sea monsoon onset time shows significant negative correlation with the South Asian High intensity (R = −0.68, p < 0.01; Fig. 5d2). This high pressure system is centered ~90°E but shifts zonally on an inter-annual basis and links the westerlies in the mid-latitudes to the easterlies in the tropics (Liu and Wu 2004). Its evolution in May is believed to bridge the Asian Summer Monsoon onset over the Bay of Bengal, the South China Sea, and the Indian sectors (Liu et al. 2013; Liu and Zhu 2016; Wu and Liu 2014). Our study supplements previous work in emphasizing the potentially close negative correlation between South China Sea monsoon onset and the South Asian High intensity (Liu and Zhu 2016), as monsoon precipitation releases latent heat to the east (Wu et al. 2015), thus contributing to atmospheric warming and the enhancement of the South Asian High. Note the distinctly strong South Asian High during June–August in 2010 (Fig. 5d), which is associated with ENSO development (Liu and Zhu 2016). Its coincidence with extremely early South China Sea monsoon onset as identified by $\delta^{18}O_p$ implies possible ENSO influence on isotopic compositions in both regions.

4.3 Impact of tropical cyclones on isotopic depletion

High resolution $\delta^{18}O_p$ data not only offer insights into monsoon variability, but also have the potential to describe

possible mechanisms that drive distinctive variations in those systems. $\delta^{18}O_p$ values are directly affected by large-scale atmospheric circulation and moisture trajectories (Sengupta and Sarkar 2006; Tian et al. 2001; Yoshimura et al. 2010). Tropical cyclones impact monsoons and regional water resources (IPCC 2013), thus their role in recent monsoon variations is of interest. These cyclones are associated with higher condensation levels and lower temperatures in the upper atmosphere (Hartmann et al. 2013). In addition, the storm-driven upwelling of cold water at the moisture source results in cooler water vapor at that location. Thus, there is a high likelihood that $\delta^{18}O_p$ in the resulting precipitation would be extremely ^{18}O depleted (which might be identified as negative outliers in Fig. 2a, b).

Tropical cyclones forming over the northern Indian and western Pacific Oceans have short life spans and relatively small radii. As shown in Fig. 6, storms in the northern Indian Ocean seldom occur during the monsoon maturation phase (June–September), and in only a few instances do they coincide with extremely depleted $\delta^{18}O_p$ values in the SETP (gray shading in Fig. 6). In contrast, extremely depleted $\delta^{18}O_p$ in the SECN are mostly coincident (in 12 out of the 18 occurrences) with typhoons that form over the western Pacific during the mature phase, although we note the lack of agreement between many western Pacific cyclone occurrences and isotopic depletion in the SECN (Fig. 6). In fact, back-trajectory studies find that the coincidences of extremely low SETP and SECN $\delta^{18}O_p$ associated with typhoons occur only when the storms made landfall within areas close to these regions, i.e., over the southern coast of Bangladesh close to the SETP, or over southeast coastal China (Fig. S5). Thus not all tropical cyclones that form over their respective oceanic moisture sources lead to extremely depleted $\delta^{18}O_p$ in their respective regions. Still, the higher coincidence of low $\delta^{18}O_p$ values in the SECN with tropical cyclones over adjacent oceans implies a much stronger impact of typhoons on the coastal region compared with inland. This can be attributed to the marine origin of these storms which weaken rapidly as they move over land and are cut off from their primary energy source (IPCC 2013).

The average atmospheric circulation during summer (June–August) features strong convection over the northeastern Bay of Bengal for the SETP and the southeastern South China Sea for the SECN (Fig. 7a). Atmospheric circulation shows the SECN under the influence of cyclonic activity, which pulls significant amounts of oceanic moisture via southwesterly airflow across the Indian peninsular, Bay of Bengal and Indo–China Peninsula (Fig. 7b). Such a circulation pattern is accompanied by significant positive correlations between $\delta^{18}O_p$ and the OLR over a small portion of the southwestern Bay of Bengal (Fig. 7b), implying a possible linkage between convection along the southwesterly trajectory and isotopic depletion in the SECN. The extremely low

$\delta^{18}O_p$ values thus might be attributed to the combination of long-distance moisture transport and local convection on coincident days (Araguas-Araguas et al. 1998; Cai and Tian 2016).

On the other hand, extremely low $\delta^{18}O_p$ in the SETP shows no significant correlation with OLR over the adjoining oceans (Fig. 7c), suggesting little direct effect of tropical cyclones in the Bay of Bengal with isotopic depletion in the SETP. Instead, the tropical cyclones may force the intense southwesterly winds further south, forming an extended transport trajectory before reaching the SETP and thus resulting in extremely low $\delta^{18}O_p$ (Gao et al. 2011; Yao et al. 2013; Yu et al. 2016). It is also worth noting that there are very few (3 out of 12) cases in which extremely low $\delta^{18}O_p$ in the SETP coincides tropical cyclones in the Bay of Bengal. The comparison thus highlights the more direct effect of tropical cyclones on the SECN than on the SETP. The centers of convection bearing significant correlations with $\delta^{18}O_p$ in the SECN shift from the southwest Bay of Bengal on days when extreme $\delta^{18}O_p$ depletion coincides with tropical cyclones occurrence (Fig. 7b), to the South China Sea on non-coincident days (Fig. 7d). The isotopic depletion during co-incident days is thus influenced by local cyclonic convection and long-distance oceanic moisture transport under the prevailing westerly jet. In cases of isotopic depletion in the absence of tropical cyclones, significant positive correlations are observed between $\delta^{18}O_p$ in the SECN and convection over the South China Sea (Fig. 7d), and between $\delta^{18}O_p$ in the SETP and convection over the northern Himalayas and Bay of Bengal (Fig. 7e), suggesting $\delta^{18}O_p$ depletion in the monsoon domain is closely affected by convective activity. The accompanying wind circulation features southwesterly warm air advecting from the oceans, which are the major moisture suppliers. The warm, moist air is uplifted and condenses to precipitate. The rise of the condensation level and decrease in condensation temperature might be instrumental in isotopic depletion during non-coincident days.

The direct influence of tropical cyclones in regions like the SETP that are farther away from the ocean is limited, which is demonstrated by fewer coincident days and no significant correlations with regional OLR during coincident days. The dramatic decreases in $\delta^{18}O_p$ are generally attributed to large-scale circulation, i.e., prevailing mid-latitude westerlies and associated long-distance transport. On days when depleted $\delta^{18}O_p$ in the SETP does not coincide with tropical cyclones in the northern Indian Ocean, there is noticeable intensification of westerly velocities. The convection fields show significant correlation with $\delta^{18}O_p$ over the Himalayas and the northern Bay of Bengal, both located in the upwind direction. The isotopic depletion in the SETP may be supplemented by low temperature along the moisture transport trajectory. Note that a large proportion of anomalously depleted $\delta^{18}O_p$ values in the SETP occurred during
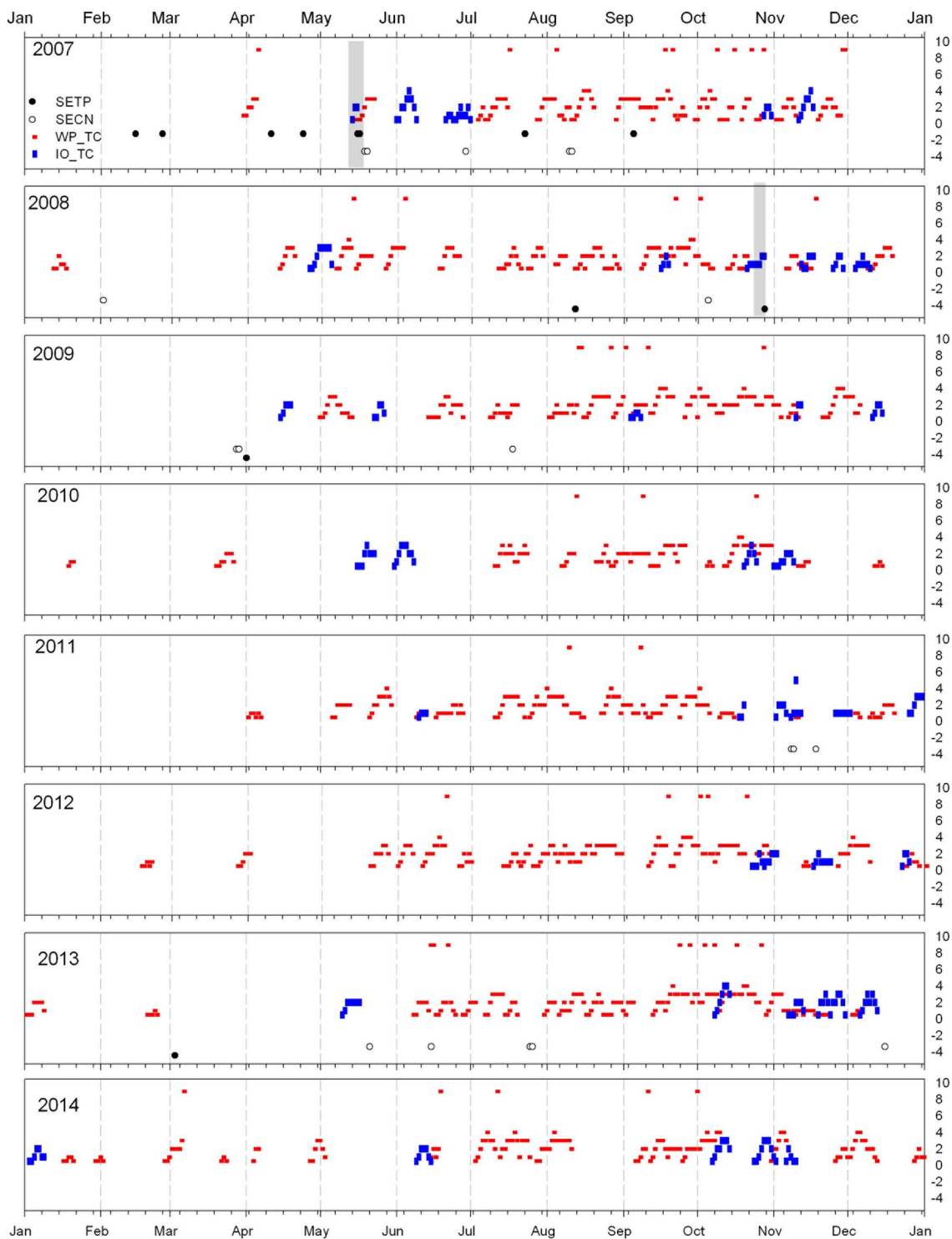
Fig. 6 Time series of anomalously depleted $\delta^{18}O_p$ occurrences in the SETP (black dots) and SECN (open circles) and their coincidences with tropical cyclones over, respectively, the northern Indian Ocean (blue dots) and the Western Pacific (red dots) from 2007 to 2014. The y-axes on the right of each panel show the intensity levels of those tropical cyclones. Gray bars highlight the limited coincidences between isotopic depletion in the SETP and tropical cyclones. Occurrences of the cyclones and their respective intensity levels are acquired through metoc.ndbc.noaa.gov/web
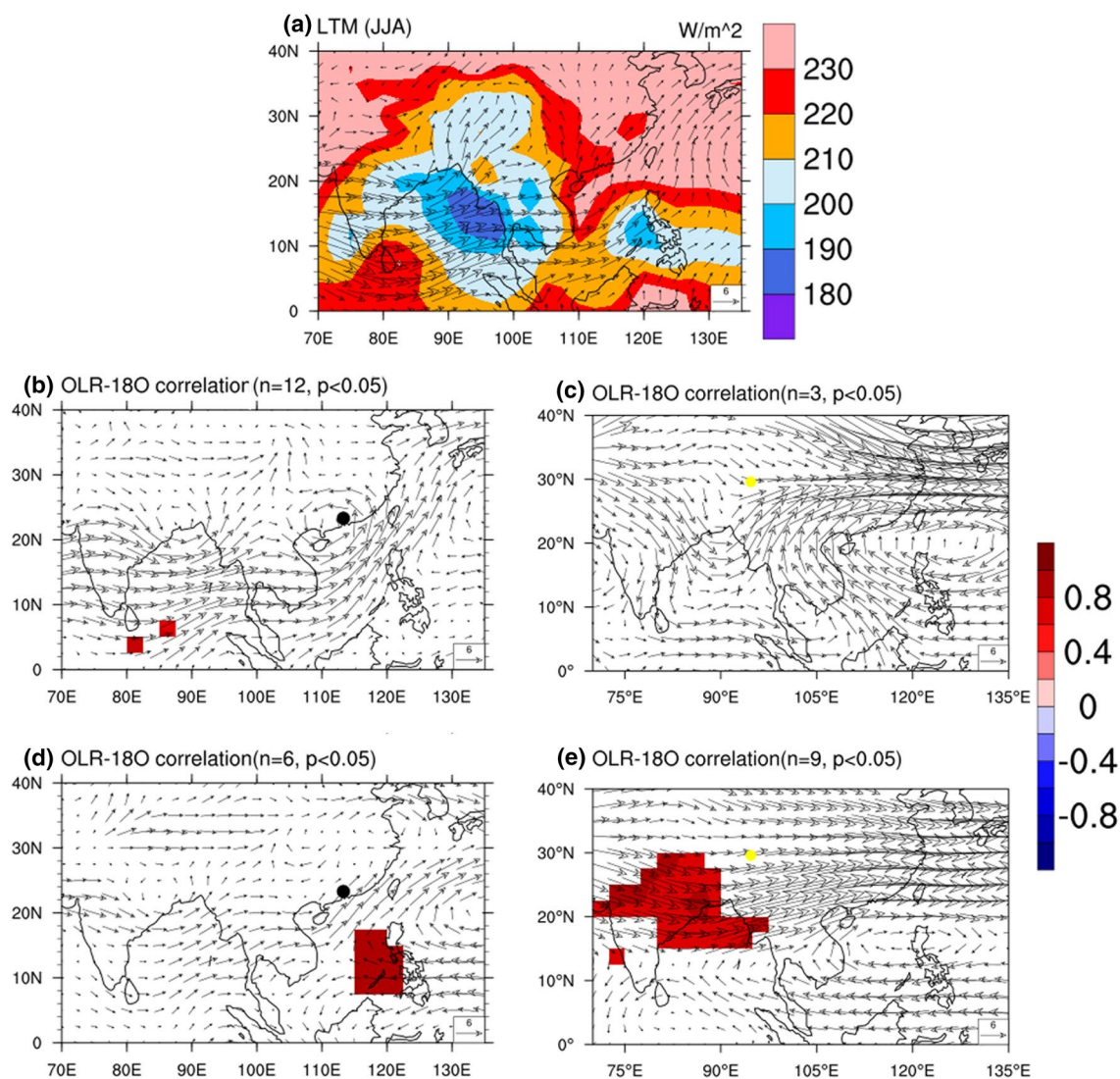
Fig. 7 Super-position of OLR fields (shaded) on wind circulation (vectors) over East Asia. **a** Average status for June–August based on the long-term mean (1981–2010); **b** composite for days of coexisting low $\delta^{18}O_p$ in the SECN and tropical cyclones over the western Pacific, **c** composite of days of coexisting low $\delta^{18}O_p$ in the SETP and tropical cyclones over northern Indian Ocean; **d** composite for days of anomalously low $\delta^{18}O_p$ in the SECN without tropical cyclones in the vicinity; **e** same as **d**, but for the SETP. Contemporaneous wind circulation vectors, which account for the elevation of the two study areas, are superimposed on all the panels, at 500 hPa for the SETP and 850 hPa for the SECN. Study sites are marked by filled circles in **b**–**e**. Shading denotes regions of significant correlation between OLR and $\delta^{18}O_p$. Daily wind velocities are from NCEP/NCAR reanalysis data (Kalnay et al. 1996) and the OLR data are from NOAA uninterpolated OLR

March–May, when both temperature and amount effects were significant, thus allowing the combined effect of low condensation temperature and long-distance transport trajectory on extremely depleted isotopic values.

4.4 Effect of water vapor transport on isotopic composition in precipitation

The flux and divergence of vertically integrated water vapor from the surface to 300 hPa (Banacos and Schultz 2005; Godfred-Spenning and Reason 2002; Konwar et al.

2012) offers insights into moisture sources and trajectory. From 2007 to 2014, the vertical integral of the divergence of water vapor over the TP shows clear seasonality, highlighting noticeable convergence over the southeastern edge of the TP from March to May and during June–August (Fig. 8). However, corresponding $\delta^{18}O_p$ values are high in the spring and low in the summer (Fig. 2). Analysis of the vertically integrated water vapor transport suggests that the distinct trajectory is the major driver of these differences. Other than summer (June–August), when the vertically integrated water vapor transport shows significant
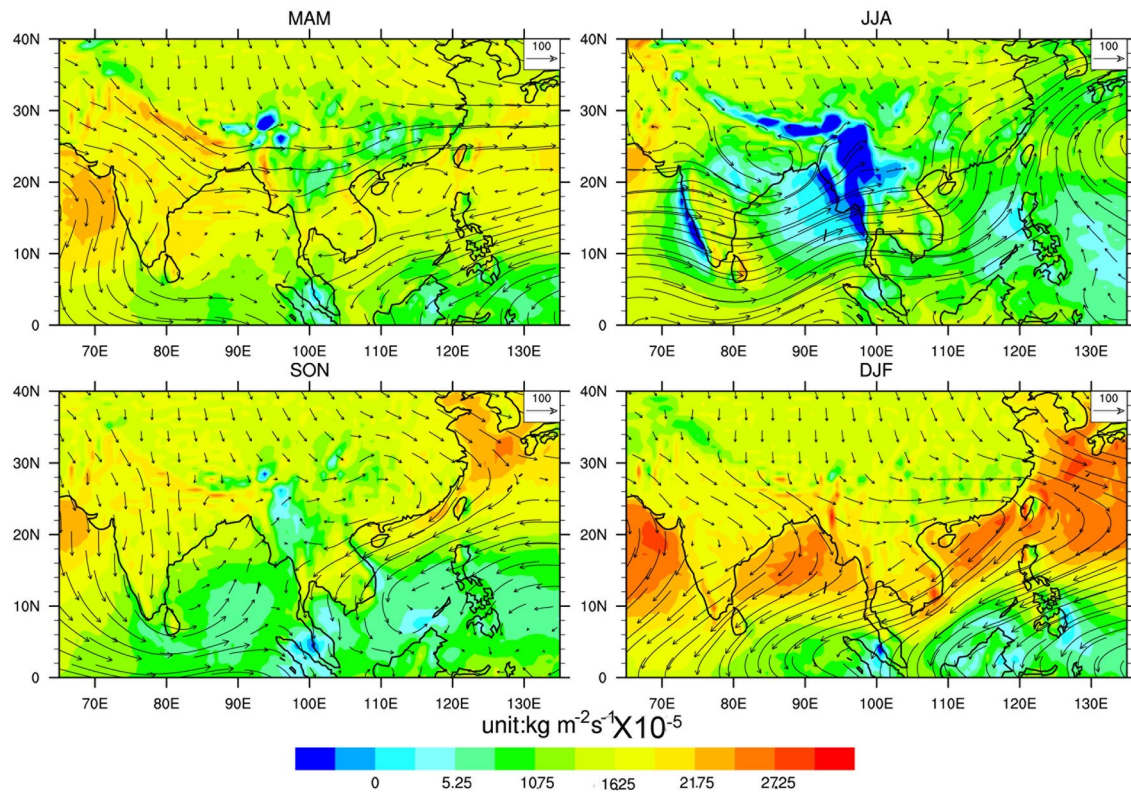
Fig. 8 Long-term mean seasonality of vertically integrated water vapor flux (curved vectors) and divergence (shaded) based on ERA-interim monthly reanalysis data from 2007 to 2014

southwesterly inflow from the northeastern Bay of Bengal, continental flow from the northwest and local circulation suggest the dominance of large-scale moisture convergence during months of monsoon convection and surface evaporation in other months. Likewise, water vapor convergence is posited to be less relevant than the vertically integrated water vapor in controlling $\delta^{18}O_p$ variations in the SECN.

Vertically integrated water vapor transport shows divergence throughout the year, however, the monthly $\delta^{18}O_p$ values display clear intra-seasonal variations, with the most negative values occurring from May to September. Correspondingly, during spring and summer, the water vapor flows from the adjacent oceans with either a regional or large-scale circulation stream, while during autumn and winter the flow is northerly from the continent. In addition, the convergence of vapor during monsoon convection will reinforce the isotopic depletion in the precipitation (Moore et al. 2014), leading to much larger spring/summer variations in amplitude in the SETP than the SECN. Thus the seasonality of $\delta^{18}O_p$ in both regions varies with: (1) the large-scale atmospheric circulation, (2) the vertically integrated water budget, and (3) convergence (divergence) and/or moisture supply from the large scale circulation prevailing over the adjacent oceans (continent) which results in low (high) isotopic values.

4.5 Interactions of snow cover variation with monsoon as indicated by $\delta^{18}O_p$

Samples were collected during precipitation events at both sites, thus the data availability reflects precipitation frequency in each region. The precipitation frequency in both regions during periods of positive Eurasian snow cover anomalies is much lower than during periods of negative anomalies (34 vs. 60 months for precipitation in the SECN, and 26 vs. 57 months for precipitation in the SETP) (Fig. 9a–d). This corresponds to a much smaller monthly precipitation amount in both regions during positive compared with negative Eurasian snow cover anomalies, i.e., 28.7 vs. 100.7 mm/month, respectively, for the SECN, and 113.7 vs. 212.9 mm/month, respectively for the SETP. This indicates a negative effect of snow cover extent over the Eurasian continent on monsoon precipitation (Wu et al. 2012; Yim et al. 2010).

Otherwise, snow cover anomalies over Eurasia show no significant correlation with $\delta^{18}O_p$ and its signal of monsoon onset in either winter or spring from 2007 to 2014. Instead, lagged correlation analysis of all monthly $\delta^{18}O_p$ anomalies in each respective region (n, the number of data points considered, is 94 for the SECN and 83 for the SETP) with corresponding Eurasian snow cover anomalies during the
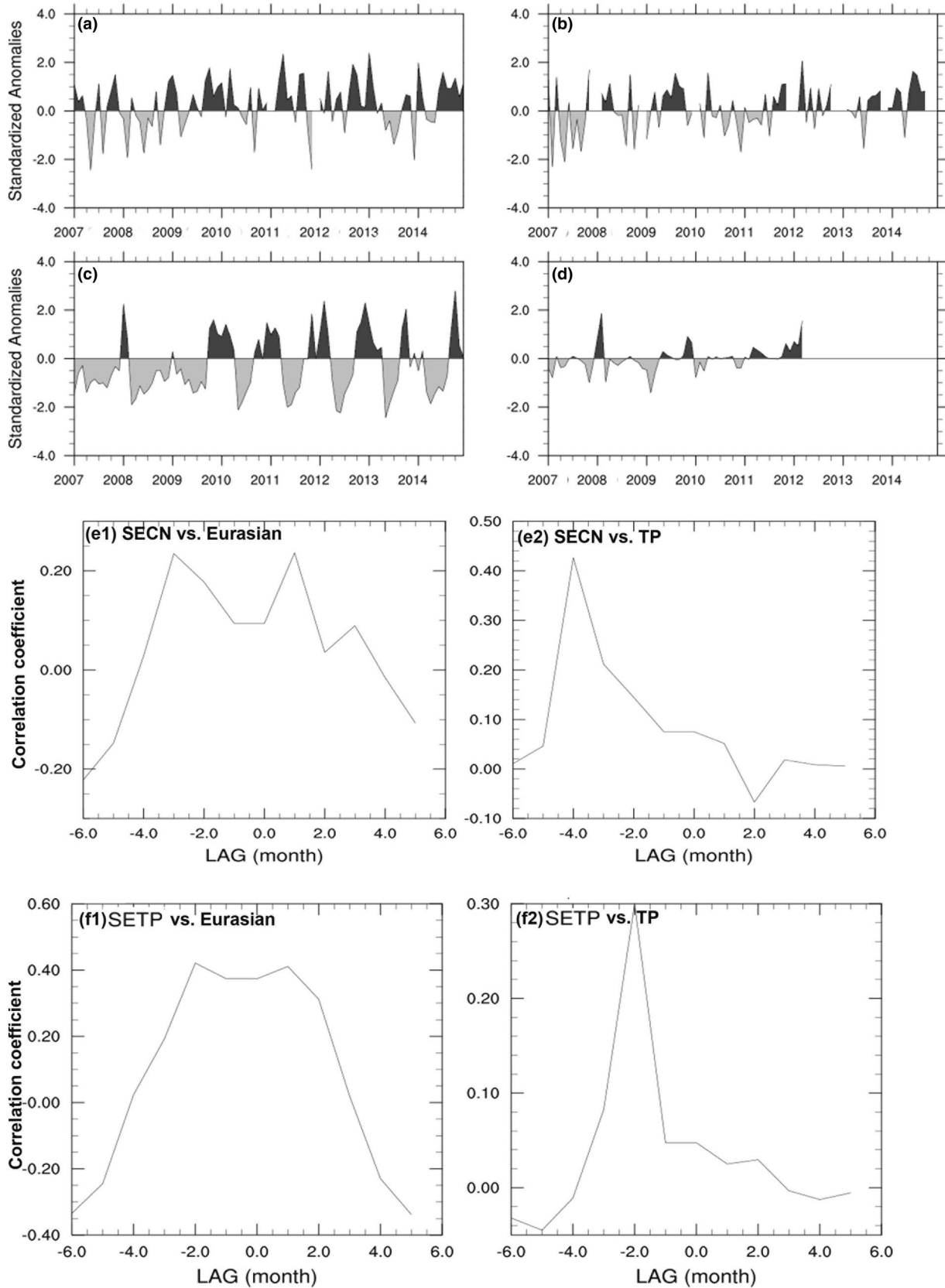
◀**Fig. 9** Monthly anomalies of $\delta^{18}O_p$ and snow cover area from 2007 to 2014, together with their lagged correlations. **a** Monthly anomalies of $\delta^{18}O_p$ in the SECN, and **b** in the SETP, **c** standardized monthly anomalies of snow cover over the Eurasian continent and **d** over the Tibetan Plateau. **e1** Lagged correlations of the SECN $\delta^{18}O_p$ anomalies with Eurasian snow cover anomalies, **e2** the same as **e1**, but using snow cover anomalies over the TP. **f1** and **f2** are the same as **e1** and **e2**, respectively, but of $\delta^{18}O_p$ anomalies in SETP. Snow cover anomalies are calculated with 1981–2010 as the base period

study period show significant relationships with a 1-month lag (Fig. 9e1, f1). This implies an overall delayed effect of Eurasian snow cover area on the subsequent monsoon circulation, which might be associated with the further westward and/or northward location and larger geographical scale of the snow cover. The lagged positive correlation between Eurasian anomalies and $\delta^{18}O_p$ in the SECN is consistent with a negative correlation between snow cover and frequency of cyclone landfall in China (Xie et al. 2005), as such an increased frequency usually contributes to monsoon intensification with deep convection, resulting in low $\delta^{18}O_p$.

In comparison, relatively stronger correlations ($p < 0.05$) exist for snow cover anomalies over TP in a certain month with monsoon onsets over both the South China Sea (Fig. S6.1) and Bay of Bengal (Fig. S6.2). It is noteworthy that snow cover over TP in May (from 2007 to 2011) shows robust positive correlations (R = 0.99, $p < 0.01$) with Bay of Bengal monsoon onset dates (Fig. S6.2). This can be attributed to slowing of the continental warming over the TP as expansive snow cover increases surface albedo, thus delaying formation of the prerequisite land-sea thermal contrast (Pu and Xu 2009). Seasonally, there is a weak negative correlation (R = − 0.80, n = 6, $p < 0.1$) between the December to February TP snow cover anomalies and subsequent summer $\delta^{18}O_p$ in the SETP, while a weak positive correlation (R = + 0.81, n = 5, $p < 0.1$) occurs between the March to May snow cover and subsequent summer $\delta^{18}O_p$ in the SECN. This suggests a "memory" effect of TP snow cover on the large-scale atmospheric circulations over Asia. Because of its high elevation and location in the mid-latitude westerly system, along with its sensible heating and thermal forcing, the TP bears a strong influence on regional climate downwind from it (Liu et al. 2012).

Anomalous monsoon rainfall is related to regional (Rajeevan 2002) and/or large-scale (Yang 1996) atmospheric circulation, and may consequently affect the snow cover extent in the region. Snow cover anomalies on the TP are positively correlated with a 3 (2)-month lag in $\delta^{18}O_p$ anomalies in the SECN (SETP) (Fig. 9e, f), suggesting responding mechanisms of snow cover anomalies over TP to Asian summer monsoon evolution. Meanwhile, aerosol loading tends to dim the solar insolation over the TP surface, thus decreasing both the continental warming and land-sea thermal contrasts which in turn weakens the South Asian Summer Monsoon

(Boos and Storelvmo 2016; Kim et al. 2016). This feedback between snow cover over the TP and Asian monsoon evolution therefore warrants further study.

5 Summary

Under a global climate change scenario, monsoon variations may be attributed to two influences: (1) the variation in atmospheric circulations associated with the land-sea thermal contrast; and (2) water vapor availability that might be attributed to sea surface warming. From the synoptic point of view, various monsoon onset criteria consider one perspective of the physical features related to the monsoon. The isotopic ratios in precipitation record the whole precipitation process, including water vapor source, transport trajectory, condensation and precipitation. As a product of an integrated system, $\delta^{18}O_p$ can be used as a reliable and commonly accepted criterion in monsoon onset evaluation. Stable isotopic depletion in precipitation coincides closely with the Asian monsoon variations. The monsoon onset timing, as determined by the isotopic criteria, generally agree with the onset timing based on the meridional temperature gradient, thus suggesting that the initially sustained isotopic depletion generally captures the major synoptic features of the Asian monsoon onset. Examination of contemporary circulation fields shows a strong link between $\delta^{18}O_p$ and 850 hPa meridional wind velocities over adjacent oceans, which is closely linked to the major moisture trajectory during the monsoon season. The southerly winds bridge the isotopic variations in both regions with monsoon circulation processes, as higher (lower) velocity southerlies coincide with more depleted (enriched) $\delta^{18}O_p$ during June–August. Weakening of the bridge in 2009 and 2014, as indicated by lower meridional wind velocities, resulted in a much delayed monsoon onset signal in daily $\delta^{18}O_p$ in both the SETP and SECN, as longer transport time is expected for the oceanic moisture to reach the continent. The South Asian High to the east of the TP is also found to contribute significantly to the inter-annual variation of monsoon onset timing over the South China Sea.

The potential effects of various phenomena on the isotopic signals of monsoon systems are explored. The occurrence of tropical cyclones is found to exert a much stronger impact on $\delta^{18}O_p$ in the SECN than in the SETP. In comparison, isotopic depletion in the SETP is attributable mainly to mid-latitude westerlies and low temperature along the upstream portion of major circulation paths. Snow cover anomalies on the TP exert a strong impact on $\delta^{18}O_p$ in both regions. A significant positive correlation is observed between snow cover anomalies in May and summer $\delta^{18}O_p$ in both regions.

Intra-seasonal variations of $\delta^{18}O_p$ in both regions are strongly affected by vertically integrated water vapor transport, with the dominance of large-scale water vapor transport contributing to isotopic depletion in the summer while surface evaporation contributes to isotopic enrichment in other months. Convergence and advection are instrumental in the dominance of large-scale circulation over regional climate in both regions.

References

Adler RF, Huffman GJ, Chang A, Ferraro R, Xie P, Janowiak J, Rudolf B, Schneider U, Curtis S, Bolvin D, Gruber A, Susskind J, Arkin P, Nelkin E (2003) The version 2 Global Precipitation Climatology Project (GPCP) monthly precipitation analysis (1979-present). J Hydrometeorol 4:1147–1167

Ananthakrishnan R, Pathan JM, Aralikatti SS (1983) The onset phase of the Southwest monsoon. Curr Sci India 52(16):755–764

Araguas-Araguas L, Froehlich K, Rozanski K (1998) Stable isotope composition of precipitation over southeast Asia. J Geophys Res Atmos 103(D22):28721–28742

Araguas-Araguas L, Froehlich K, Rozanski K (2000) Deuterium and oxygen-18 isotope composition of precipitation and atmospheric moisture. Hydrol Process 14(8):1341–1355

Banacos PC, Schultz DM (2005) The use of moisture flux convergence in forecasting convective initiation: historical and operational perspectives. Weather Forecast 20(3):351–366

Benetti M et al (2014) Deuterium excess in marine water vapor: dependency on relative humidity and surface wind speed during evaporation. J Geophys Res Atmos 119(2):584–593

Boos WR, Storelvmo T (2016) Near-linear response of mean monsoon strength to a broad range of radiative forcings. Proc Natl Acad Sci USA 113(6):1510–1515

Cai ZY, Tian LD (2016) Atmospheric controls on seasonal and interannual variations in the precipitation isotope in the East Asian monsoon region. J Climate 29(4):1339–1352

Clark I, Fritz P (1997) Environmental isotopes in hydrogeology. Lewis Publishers, Ann Arbor

Conroy JL, Overpeck JT (2012) Regionalization of present-day precipitation in the greater monsoon region of Asia (vol 24, pg 4073, 2011). J Climate 25(2):815–817

Dansgaard W (1964) Stable isotopes in precipitation. Tellus 16(4):436–468

Froehlich K et al (2008) Deuterium excess in precipitation of Alpine regions—moisture recycling. Isot Environ Health Stud 44(1):61–70

Gao J et al (2011) Precipitation water stable isotopes in the South Tibetan Plateau: observations and modeling. J Climate 24(13):3161–3178

Gat JR et al (1996) The stable isotope composition of waters of the eastern Mediterranean Sea. J Geophys Res Oceans 101(C3):6441–6451

Gat JR (2005) Some classical concepts of isotope hydrology:"Rayleigh fractionation, Meteoric Water Lines, the Dansgaard effects (altitude, latitude, distance from coast and amount effects) and the dexcess parameter". In: Aggarwal PK, Gat JR, Froehlich K.F.O. (eds) Isotopes in the Water Cycle:, Present and Future of a Developing Science. IEA, Amsterdam, pp 127–137

Godfred-Spenning CR, Reason CJC (2002) Interannual variability of lower-tropospheric moisture transport during the Australian monsoon. Int J Climatol 22(5):509–532

Goswami BN, Jayavelu V (2001) On possible impact of the Indian summer monsoon on the ENSO. Geophys Res Lett 28(4):571–574

Goswami BN, Krishnamurthy V, Annamalai H (1999) A broad-scale circulation index for the interannual variability of the Indian summer monsoon. Q J Roy Meteor Soc 125(554):611–633

Guo QY (1983) The summer monsoon intensity index in East Asia and its variation. Acta Geogr Sin 38(3):11

Hartmann DL et al (2013) Observations: Atmosphere and Surface. In: Stocker TF et al (eds) Climate change 2013: the physical science basis. Constribution of Working Group I to the Fifth Assessment Report of the Integovernmental Panel on Climate Change. Cambridge University Press, Cambridge

IPCC (2013) Climate change 2013: the physical science basis. In: Contribution of working group I to the fifth assessment report of the intergovernmental panel on climate change. Cambridge University Press, Cambridge, New York, NY, pp 1535

Johnson KR, Ingram BL (2004) Spatial and temporal variability in the stable isotope systematics of modern precipitation in China: implications for paleoclimate reconstructions. Earth Planet Sci Lett 220(3–4):365–377

Kalnay E et al (1996) The NCEP/NCAR 40-year reanalysis project. B Am Meteorol Soc 77(3):437–471

Kim MJ, Yeh SW, Park RJ (2016) Effects of sulfate aerosol forcing on East Asian summer monsoon for 1985–2010. Geophys Res Lett 43(3):1364–1372

Konwar M, Parekh A, Goswami BN, 2012. Dynamics of east-west asymmetry of Indian summer monsoon rainfall trends in recent decades. Geophys Res Lett, 39

Kurita N (2013) Water isotopic variability in response to mesoscale convective system over the tropical ocean. J Geophys Res Atmos 118(18):10376–10390

Lau KM, Yang S (1996) Seasonal variation, abrupt transition, and intraseasonal variability associated with the Asian summer monsoon in the GLA GCM. J Climate 9(5):965–985

Liu YM et al (2012) Revisiting Asian monsoon formation and change associated with the Tibetan Plateau forcing: II. Change. Clim Dyn 39(5):1183–1195

Liu ZF, Tian L, Yao TD, Yu WS (2008) Seasonal deuterium excess in Nagqu precipitation: influence of moisture transport and recycling in the middle of Tibetan Plateau. Environ Geol 55(7):1501–1506

Liu YM, Wu GX (2004) Progress in the study on the formation of the summertime subtropical anticyclone. Adv Atmos Sci 21(3):322–342

Liu BQ, Wu GX, Mao JY, He JH (2013) Genesis of the South Asian High and its impact on the Asian Summer monsoon onset. J Climate 26(9):2976–2991

Liu BQ, Zhu CW (2016) A possible precursor of the South China Sea summer monsoon onset: Effect of the South Asian High. Geophys Res Lett 43(20):11072–11079

Liu JR, Song XF, Yuan GF, Sun XM, Yang LH, 2014. Stable isotopic compositions of precipitation in China. Tellus Ser B Chem Phys Meteorol 66:22567

Mao JY, Chan JCL, Wu GX (2011) Interannual variations of early summer monsoon rainfall over South China under different PDO backgrounds. Int J Climatol 31(6):847–862

Moore M, Kuang Z, Blossey PN (2014) A moisture budget perspective of the amount effect. Geophys Res Lett 41(4):1329–1335

Parthasarathy B, Kumar KR, Kothawale DR (1992) Indian-Summer Monsoon Rainfall Indexes—1871–1990. Meteorol Mag 121(1441):174–186

Pu ZX, Xu L (2009) MODIS/Terra observed snow cover over the Tibet Plateau: distribution, variation and possible connection with the East Asian Summer Monsoon (EASM). Theor Appl Climatol 97(3–4):265–278

Qian W, Yang S (2000) Onset of the regional monsoon over Southeast Asia. Meteorol Atmos Phys 75(1–2):29–38

Rajeevan M (2002) Winter surface pressure anomalies over Eurasia and Indian summer monsoon. Geophys Res Lett 29(10):1454. http://dx.doi.org/10.1029/2001GL014363

Risi C, Bony S, Vimeux F (2008) Influence of convective processes on the isotopic composition (delta O-18 and delta D) of precipitation and water vapor in the tropics: 2. Physical interpretation of the amount effect. J Geophys Res Atmos 113:D19

Robinson DA, Estilow TW, Program NC, 2012. NOAA climate data record (CDR) of Northern Hemisphere (NH) snow cover extenet (SCE), version 1: Eurasia monthly. NOAA National Climatic Data Center, Asheville

Sengupta S, Sarkar A (2006) Stable isotope evidence of dual (Arabian Sea and Bay of Bengal) vapour sources in monsoonal precipitation over north India. Earth Planet Sci Lett 250(3–4):511–521

Shen SSP et al (2015) Characteristics of the Tibetan Plateau snow cover variations based on daily data during 1997–2011. Theor Appl Climatol 120(3–4):445–453

Singh D (2016) Tug of war on rainfall changes. Nat Clim Change 6:20–22

Tian L, Masson-Delmotte V, Stievenard M, Yao T, Jouzel J (2001) Tibetan Plateau summer monsoon northward extent revealed by measurements of water stable isotopes. J Geophys Res Atmos 106(D22):28081–28088

Trenberth KE (2011) Changes in precipitation with climate change. Climate Res 47(1–2):123–138

Wallace JM, Hobbs PV (1977) Atmospheric sciences: an introductory survey. Academic Press, New York

Wang B, Fan Z (1999) Choice of south Asian summer monsoon indices. B Am Meteorol Soc 80(4):629–638

Wang B, Kang IS, Lee JY (2004b) Ensemble simulations of Asian-Australian monsoon variability by 11 AGCMs. J Climate 17(4):803–818

Wang B, LinHo LH (2002) Rainy season of the Asian-Pacific summer monsoon. J Climate 15(4):386–398

Wang B, LinHo LH, Zhang YS, Lu MM (2004a) Definition of South China Sea monsoon onset and commencement of the East Asia summer monsoon. J Climate 17(4):699–710

Webster PJ, Yang S (1992) Monsoon and Enso - Selectively Interactive Systems. Q J Roy Meteor Soc 118(507):877–926

Wu GX et al (2011) Vortex genesis over the Bay of Bengal in spring and its role in the onset of the Asian Summer Monsoon. Sci China Earth Sci 54(1):1–9

Wu GX, He B, Liu YM, Bao Q, Ren RC (2015) Location and variation of the summertime upper-troposphere temperature maximum over South Asia. Clim Dyn 45(9–10):2757–2774

Wu RG, Kirtman BP (2007) Observed relationship of spring and summer East Asian rainfall with winter and spring Eurasian snow. J Climate 20(7):1285–1304

Wu ZW, Li JP, Jiang ZH, Ma TT (2012) Modulation of the Tibetan plateau snow cover on the ENSO teleconnections: from the East Asian summer monsoon perspective. J Climate 25(7):2481–2489

Wu GX, Liu BQ (2014) Roles of forced and inertially unstable convection development in the onset process of Indian summer monsoon. Sci China Earth Sci 57(7):1438–1451

Wu GX, Zhang YS (1998) Tibetan Plateau forcing and the timing of the monsoon onset over South Asia and the South China Sea. Mon Weather Rev 126(4):913–927

Wushiki H, et al (1993) Isotope hydrological features of the Tarim Basin, China. In: Proceedings of the Japan-China international symposion on the study of the mechanism of desertification. Tsukuba, p. 380ff

Xavier PK, Marzin C, Goswami BN (2007) An objective definition of the Indian summer monsoon season and a new perspective on the ENSO-monsoon relationship. Q J Roy Meteor Soc 133(624):749–764

Xie L, Yan TZ, Pietrafesa LJ, Karl T, Xu XD (2005) Relationship between western North Pacific typhoon activity and Tibetan Plateau winter and spring snow cover. Geophys Res Lett 32(16)

Xu BQ et al. (2009) Black soot and the survival of Tibetan glaciers. Proc Natl Acad Sci USA 106(52): 22114–22118

Yang S (1996) ENSO-snow-monsoon associations and seasonal-interannual predictions. Int J Climatol 16(2):125–134

Yang XX et al (2012b) Isotopic signal of earlier summer monsoon onset in the Bay of Bengal. J Climate 25(7):2509–2516

Yang XX, Xu BQ, Yang W, Qu DM (2012a) The Indian monsoonal influence on altitude effect of delta O-18 in surface water on southeast Tibetan Plateau. Sci China Earth Sci 55(3):438–445

Yang XX, Yao TD, Yang WL, Yu WS, Qu DM (2011) Co-existence of temperature and amount effects on precipitation delta O-18 in the Asian monsoon region. Geophys Res Lett 38:L21809. http://dx.doi.org/10.1029/2011GL049353

Yao TD et al (2013) A review of climatic controls on delta O-18 in precipitation over the Tibetan Plateau: observations and simulations. Rev Geophys 51(4):525–548

Yim SY, Jhun JG, Lu RY, Wang B (2010) Two distinct patterns of spring Eurasian snow cover anomaly and their impacts on the East Asian summer monsoon. J Geophys Res Atmos 115:D22113. http://dx.doi.org/10.1029/2010JD013996

Yoshimura K, Kanamitsu M, Dettinger M (2010) Regional downscaling for stable water isotopes: a case study of an atmospheric river event. J Geophys Res Atmos:115

Yu WS et al (2016) Short-term variability in the dates of the Indian monsoon onset and retreat on the southern and northern slopes of the central Himalayas as determined by precipitation stable isotopes. Clim Dyn 47(1–2):159–172

Yurtsever E, Moreshead J, Shillady D (1975) Semiempirical natural orbital analysis of bonding and rotational energy barrier in cyclopropylmethyl cation. Chem Phys Lett 36(3):365–368

Zhou TJ et al (2009) The CLIVAR C20C project: which components of the Asian-Australian monsoon circulation variations are forced and reproducible? Clim Dyn 33(7–8):1051–1068